Atmos. Chem. Phys. Discuss., https://doi.org/10.5194/acp-2018-95
Manuscript under review for journal Atmos. Chem. Phys.
Discussion started: 3 April 2018
© Author(s) 2018. CC BY 4.0 License.

Atmospheric Chemistry and Physics Discussions

An overview on the airborne measurement in Nepal,-part 1: vertical profile of aerosol size-number, spectral absorption and meteorology

Ashish Singh[1]*, Khadak S. Mahata[1], Maheswar Ruphaketi[1]*, Wolfgang Junkermann[2], Arnico K. Panday[3], Mark G. Lawrence[1]

[1]Institute for Advanced Sustainability Studies, Potsdam, Germany
[2]Institute of Meteorology and Climate Research, IMK-IFU, Garmisch-Partenkirchen, Germany
[3]International Centre for Integrated Mountain Development (ICIMOD), Lalitpur, Nepal

*Corresponding author: Ashish Singh (ashish.singh@iass-potsdam.de) and Maheswar Rupakheti (maheswar.rupakheti@iass-potsdam.de)

Atmos. Chem. Phys. Discuss., https://doi.org/10.5194/acp-2018-95
Manuscript under review for journal Atmos. Chem. Phys.
Discussion started: 3 April 2018
© Author(s) 2018. CC BY 4.0 License.

Atmospheric Chemistry and Physics Discussions

Abstract

The paper provides an overview of an airborne measurement campaign with a microlight aircraft, over the Pokhara Valley region, Nepal, a metropolitan region in the central Himalayan foothills. This is the first aerial measurements in the central Himalayan foothill region, one of the polluted but relatively poorly sampled regions of the world. Conducted in two phases (in May 2016 and December 2016-January 2017), the goal of the overall campaign was to quantify the vertical distribution of aerosols over a polluted mountain valley in the Himalayan foothills, as well as to investigate the extent of regional transport of emissions into the Himalayas. This paper summarizes results from first phase where test flights were conducted in May 2016 (pre-monsoon), with the objective of demonstrating the potential of airborne measurements in the region using a portable instrument package (size with housing case: 0.45 m x 0.25 m x 0.25 m, 15 kgs) onboard an ultralight aircraft (IKARUS-C42). The limited dataset collected during the test flight also provides useful insights into the impact of regional emissions and meteorology on aerosol vertical profiles. A total of five sampling test flights were conducted (each lasting for 1-1.5 h) in the Pokhara Valley to characterize vertical profiles of aerosol properties such as aerosol number and size distribution (0.3-2 µm), total particle concentration (>14 nm), aerosol absorption (370-950 nm), black carbon (BC), and meteorological variables.

The vertical profiles of aerosol species showed decreasing concentrations with altitude (815 to 4500 m a.s.l.); steep concentration gradient below 2000 m (a.s.l.) in the morning and a more mixed profiles (up to ca. 4000 m a.s.l.) in the afternoon. The strong gradient in the morning hours was mainly contributed by the primary emissions from the valley floor, including occasional open agriculture burning. The near-surface (<1000 m a.s.l.) BC concentrations observed in the Pokhara Valley were much lower than pre-monsoon BC concentrations in the Kathmandu Valley, and similar in range to Indo-Gangetic Plain (IGP) sites such as Kanpur in India. The sampling test flight also detected an elevated polluted aerosol layer (around 3000 m a.s.l.) over the Pokhara Valley, which could be associated with the regional transport. The total aerosol and black carbon concentration in the polluted layer was comparable with the near-surface values (<1000 m a.s.l.). The elevated polluted layer was also characterized by high aerosol extinction co-efficient (at 550 nm) and was identified as smoke and a polluted dust layer. Long-term observations of aerosol optical depth (AOD) in the Pokhara Valley (2010-16) showed strong seasonality, with a pre-monsoon maximum which is also indicative of westerly advection transporting a mixture of dust and other aerosols from IGP into Himalayan foothills and mountain valleys. The observed shift in the westerlies (at 20-30° N) entering Nepal during the test flight

© Author(s) 2018. CC BY 4.0 License.

period is an important factor for the presence of elevated polluted layers in the Pokhara Valley. The intrusions (in the form of a trough) of the cold and humid air mass from the mid-latitude (~ 40-50° N) a shift in the direction of synoptic airmass entering Himalayas. This synoptic-scale interaction is likely to drive the transport into the mountain valleys and higher Himalayas.

1. Introduction

The Himalayas and surrounding regions are one of the unique ecosystems in the world, with a great variety in the geography and socio-economics, and a notable significance in the context of regional and global environmental change. Areas in the foothills of the Himalayas still constitute large regions of rural populations along with pockets of rapidly growing cities. Consequently, there is a complex interaction among changing emission sources and their interaction with regional and global climate change. Among emitted air pollutants, the chemical and physical properties of aerosols have been linked to significant burdens of disease, to melting of glaciers, to crop loses, to hydrological changes and to cloud properties (Bollasina et al., 2011;Vinoj et al., 2014;Lau, 2014;Burney and Ramanathan, 2014;Brauer et al., 2012;Cong et al., 2015;Li et al., 2016).

Sources of aerosols in the Himalayas and the nearby Indo-Gangetic Plain (IGP) typically vary between urban, peri-urban and rural locations; fossil fuel and industrial emissions such as vehicles, brick kilns, waste burning, cement factories etc., are typically urban and peri-urban; biomass cookstove, agriculture and waste burning and forest fires are often linked to emissions from rural areas (Guttikunda et al., 2014;Venkataraman et al., 2006;Stone et al., 2010). Secondary chemical pathways also contribute to the aerosols in the ultrafine and accumulation-mode range via particle formation events (Venzac et al., 2008).

Aerosol properties in the Himalayas have large spatial and temporal variations, especially in the pre-monsoon and monsoon season. These observed variations are influenced by emission sources, regional meteorology and geography (Dey and Di Girolamo, 2010). The influence of aerosol particles on local and regional weather during these adjacent seasons has significant implications for timing, intensity and spatial distribution of the summer monsoon in the region (Bollasina et al., 2011;Ramanathan et al., 2001). Studies describing the aerosol-meteorology interaction are often missing in the Himalayan region partly due to lack of surface and airborne measurements of aerosol properties along with meteorology. Most past campaign-mode measurements in the Himalayan regions, to our knowledge, have been ground measurements, which have aided in evaluating aerosol properties, and their transformation and transport mechanisms (Shrestha et al., 2013;Shrestha et al., 2010;Ramana et al., 2004;Marcq et al., 2010;Panday and Prinn, 2009;Cho et al., 2017). Long-term continuous measurements of aerosols and

© Author(s) 2018. CC BY 4.0 License.

meteorology are limited to a few stations in the High Himalayas, such as the recently discontinued Nepal Climate Observatory at Pyramid (NCO-P, 27.95° N, 86.81° E, 5050 m a.s.l.), a high altitude observatory located near basecamp of Mt. Everest. Columnar and satellite measurements such as AERONET and CALIPSO have provided a regional overview of aerosol type and vertical distribution, as well as estimation of aerosol heating rate in the atmospheric column (Kuhlmann and Quaas, 2010;Gautam et al., 2011;Pandey et al., 2017).However, these measurement techniques often suffer from large uncertainty and biases while retrieving the complex nature of the aerosols observed in the region (Jai Devi et al., 2011).

Regional meteorology in the 850-500 mb range plays an important role in the transformation and transport of aerosols from Western Asia to the IGP, the Himalayan foothills, the Himalayan and Tibetan Plateau region (Decesari et al., 2010;Marinoni et al., 2013;Lüthi et al., 2015). At these altitudes, synoptic- scale air masses are mostly westerly/northwesterly during the pre-monsoon and southwesterly/easterly during the monsoon. These air masses are often linked to dust aerosol transport during the pre-monsoon season from Western Asia into the Himalayas, including populated mountain valley such as Kathmandu and Pokhara Valley in Nepal. The transported dust aerosol also mixes with the primary emission (or anthropogenic aerosols) in the IGP and accumulates from northern to eastern IGP along the Himalayan foothills (Gautam et al., 2009b;Gautam et al., 2011). The total aerosol loading is often highest during the pre-monsoon season in the IGP (Gautam et al., 2009a;Raatikainen et al., 2014), intensified further by weak surface/zonal winds and numerous open biomass burning and forest fires events (Kaskaoutis et al., 2012b). The polluted aerosol layer in the IGP is advected into the Himalayas by synoptic-scale westerlies (~500 mb) and also by the valley wind circulation within or along the planetary boundary layer (PBL) (Lüthi et al., 2015). The advection is also facilitated by strong updraft and PBL expansion (highest in the pre-monsoon in the IGP) often mixing with the synoptic-scale westerlies (Raatikainen et al., 2014). Because of strong convective activity in the IGP, the polluted air masses near the surface are often lifted up to 5-7 km or higher (Kuhlmann and Quaas, 2010). In addition to the synoptic-scale transport, thermally-driven valley winds also enable the transport of humid and polluted air mass (with enhanced absorbing fraction) from IGP into the Himalayan foothills, and further up into the mountain valleys and elevated locations (Raatikainen et al., 2014;Lüthi et al., 2015;Gogoi et al., 2014;Putero et al., 2014;Decesari et al., 2010;Marcq et al., 2010). Strongly coupled with the expansion of the PBL in the IGP, the upslope movement of polluted air masses into the foothills and further east is characterized by late afternoon peaks in AOD many measurement sites along the Himalayan range such as Hanle Valley (Ladakh, India), Mukteswar and Manora site (Nainital, India), Hetauda (Nepal), Langtang

© Author(s) 2018. CC BY 4.0 License.

Valley (Nepal), Dhulikhel (Nepal), Kathmandu Valley (Nepal) and NCO-P (Nepal). The temporal and spatial extent of this observed "ventilation" at multiple locations could be indicative of a regional-scale transport than mesoscale (Gogoi et al., 2014;Raatikainen et al., 2014;Gautam et al., 2011;Putero et al., 2015;Marcq et al., 2010).

To date there have been no observations of vertical distributions of aerosol and gaseous species carried out in the Himalayan region. Therefore, the airborne measurement campaign was designed to address two major questions: (i) what is the variation in the aerosol properties, notably the vertical distributions, over a polluted mountain valley, and (ii) what is the quantitative extent of regional transport of aerosols in the higher Himalayas? The campaign was carried out in two phases in the Pokhara Valley and surrounding areas in Nepal. In the first phase, test flights were conducted in May 2016 and in the second phase, intensive sampling flights were carried out in December 2016-January 2017. This paper provides an overview of the measurement campaign and results from the test flights in May 2016 which include snapshots of vertical profiles of aerosol size, number, and composition, along with meteorological parameters. The airborne measurements presented in this paper are supplemented with observations of local and regional meteorology, as well as satellite and ground-based column-integrated aerosol microphysics and radiative properties (see section 3.1.1 and 3.1.2). A companion paper will follow with more detailed observations and results based on the intensive measurements carried out during December 2016-January 2017.

2. Ultralight measurements in Nepal

2.1. Details of airborne measurement unit

A single-engine two-seater microlight aircraft (IKARUS C-42, COMCO IKARUS, Germany) was used as the aerial platform. The technical specification of the aircraft includes approximately 4 h of flying time, a short take-off run, an additional payload of up to 50 kg, and is suitable for spiral movement in the air. The aircraft has a cruising speed of 165 kmh^{-1}, and a 5-6 ms^{-1} rate of climb which makes it an appropriate aerial vehicle to perform measurements at altitudes within the PBL and as close as 50 m above ground level. More detail about the aircraft is available here (http://www.comco-ikarus.de/Pages/c42a-technik.php?lang=en). Its size, speed and maneuverability offered a decent climb to the free troposphere to capture vertical profiles in the rough terrains of Nepal. The aircraft used for the study is operated by the Pokhara Ultralight Company for recreational flights around the Pokhara Valley.

© Author(s) 2018. CC BY 4.0 License.

The instrument package was specifically designed and tested for aerial measurements (Junkermann, 2001). Table 1 describes each instrument and the integration performed to prepare the package for the aerial deployment. The instrument package consists of a GRIMM 1.108 for particle size distributions (0.3 to 20 µm, 16 size bins) with sampling frequency of 6 s, and a TSI CPC 3760 for total particle concentration (>11 nm) at 1 s resolution (See Figure S1 in the supplement). The package also included a Magee Scientific aethalometer (AE42) for aerosol absorption at seven different wavelengths (370 -1020 nm). The instruments were reduced in weight for use on the aircraft. The CPC was operated with a constant mass flow and an internal DC pump instead of the original flow regulation by a critical orifice. Meteorological parameters including temperature and dew point were sampled at a rate of 1 s or higher. All the sensors were connected to a modular computer (PC104) for data acquisition. The PC104 is also equipped with a Global Positioning System (GPS), and multiple serial and analog connectors. For inflight instrument checks and quick online overview of the atmospheric conditions, a small LCD was also connected to the PC104 and placed in the cockpit areas for the flight crew. This display showed real-time aerosol number concentrations and meteorological parameters.

Table 1. Instrument package deployed in the microlight aircraft

The instrument package weighs approximately 15 kg and consumes <60 W, well within the power supply range of the aircraft battery. It is housed in an aluminum box (0.45 m x0.25 mx0.25 m), and can be easily integrated with a mobile platform such as the IKARUS (See Figure S1). In IKARUS, the instrument was placed in the rear section behind the seats which is otherwise almost empty, and only contains the fuel tank and supporting aluminum bars. The sample inlet line (internal diameter of 0.004 m or ~4.0 mm ID brass tubing) ran along the wingspan and was approximately 1.8 m from the cockpit. Once the sample line is inside the aircraft, it is distributed to all the aerosol instruments using a simple metal flow splitter (0.006 m ID). The sample inlet positioning at the end of the wingspan also minimizes the influence of the aircraft propeller, located in the front of the cockpit.

2.2. Site description

Pokhara Valley is Nepal's second largest populated valley (pop. >250,000) after the Kathmandu Valley (CBS, 2011). The valley is approximately at 815 m (a.s.l.), ~150 km west of the Kathmandu Valley, and ~90 km northeast of the southern plains (~100 m a.s.l.) bordering IGP. The valley is surrounded by mountains which are approximately 1000-2000 m (a.s.l.). Further north of the Pokhara Valley, within 30 km the elevation gradient increases rapidly to over 7000 m (a.s.l.) or higher (see Figure 1). This steep

© Author(s) 2018. CC BY 4.0 License.

elevation gradient is conducive for the orographic lift of humid air masses, and thus the valley also receives one of the highest rates of precipitation in Nepal and occasional strong convective updrafts leading to hailstorms and thunderstorms (Aryal et al., 2015). The mixing of dry westerly air masses with heated moist air masses from the Bay of Bengal produces strong convection over the Pokhara Valley, and thus results in strong updrafts. These strong convective activities are frequent in the pre-monsoon and monsoon season, but do not occur during the winter season.

2.3. Test flight patterns over the Pokhara Valley

Five test flights were conducted in the morning and evening period around Pokhara Valley (83.97° E, 28.19° N, 815 m a.s.l.) with each flight lasting for about 1 to 1.5 h from 5-7th May 2016. The flight pattern was consistently flown over the northwest part of the valley (Figure 1). A typical flight would commence from the Pokhara Regional Airport (818 m a.s.l.) and steadily fly 5-10 km northwest along the Pokhara Valley toward the Himalayas. This was followed by the spiral up and down sampling from approximately 1000 to 4000 m, often reaching close to the lower base of the cloud in the free troposphere. Further climbs into the cloud layer were avoided during the test flights.

Figure 1. A typical test flight within the Pokhara Valley on 5th May 2017. The plot is generated using a Matlab-Google Earth toolbox (https://www.mathworks.com/matlabcentral/fileexchange/12954-google-earth-toolbox). Each dot is a single sample point (sampling frequency of 1Hz); the color of the dot indicates the total aerosol concentration and the value of each color is shown as a color bar.

2.4. Data processing and quality

The data from all the instruments is synced with the GPS clock, and the PC104 receives all the data simultaneously and creates a common time-stamped data file. Prior to each test flight, a zero test was conducted to identify any possible leaks in the sample line.

The collected data from the five test flights went through multiple steps of cleaning and flagging. Occasionally during the radio communication by the pilot with the ground station or air traffic controller, the CPC and the temperature sensor would record exceedingly high values. This noise is an interference picked up by the sensor from the 5 W radio transmission. The CPC and aethalometer is also sensitive to vibration in the aircraft, especially during upward and downward spiral motion, which may result in flow imbalance in these analyzers. This resulted in random noise segments for few seconds in the data, which were flagged.

Atmos. Chem. Phys. Discuss., https://doi.org/10.5194/acp-2018-95
Manuscript under review for journal Atmos. Chem. Phys.
Discussion started: 3 April 2018
© Author(s) 2018. CC BY 4.0 License.

Atmospheric Chemistry and Physics Discussions

3. Results

3.1. General meteorology and air quality, aerosol properties in the Pokhara Valley

3.1.1. Local and synoptic meteorology in the Pokhara Valley

Climatologically, Pokhara Valley has a humid subtropical climate, characterized by a summer monsoon season from late June to September, preceded by a dry pre-monsoon (March-May, see Figure S2 in the supplement). Average monthly values of commonly measured meteorological parameters, shown in Figure S2 for 2016, are similar to the in range and variations observed in other studies (Poudyal et al., 2014;Khadka and Ramanathan, 2013). The annual mean temperature in the valley was 22° C, with the lowest monthly mean in January (~15° C) and the highest in July (~ 25° C). Rainfall was also highest in the months of August and September (summer monsoon season), followed by relatively dry post-monsoon (October-November) and winter period (December-February). The late pre-monsoon to summer monsoon were also the periods of maximum monthly solar insolation (~900 Wm^{-2}) and the insolation is approximately half (~550 Wm^{-2}) during the winter. The dominant local/surface winds in the Pokhara Valley were from southeast and southwest followed by the northwest. The wind speed has a strong diurnal variability in the valley (Aryal et al., 2015) with low wind speed (<2.0 ms^{-1}) before noon-time, usually from southeast, followed by stronger winds from the southwest and northwest (>2.4 ms^{-1}) which can continue until late night. The increased wind speed in the afternoon could be katabatic in nature as a result of differential heating in the mountain valley slopes and could be linked to pollution transport from surrounding regions (Gautam et al., 2011). Winds in May 2016 were predominantly from the southeast with occasional strong winds from the southwest (see Figure S3 in the supplement). During the test flight period (5-7th May 2016), the wind was similar in directionality, with an hourly mean wind speed of 1.8 to 3.0 ms^{-1}.

Three dominant synoptic meteorology regimes characterize the seasonality of South Asia (Lawrence and Lelieveld, 2010). They are summer (June-September), the winter monsoon (mid-November to February) and the monsoon-transition periods, which include the pre-monsoon season (March-May) and post-monsoon season (mid-September to mid-November). These synoptic regimes are also active in the Himalayas, including the Pokhara Valley. The monsoon transition period, during which the test flights measurements were conducted, is characterized by westerlies over 20-30° N at 850 mb and above (see Figure 2). Figure 2 shows the daily wind vector over South Asia for 3, 5, 6 and 7 May 2016 generated using the NCEP NCAR Reanalysis data at 2.5°x 2.5° horizontal resolution. While the reanalysis data can be expected to represent the synoptic-scale phenomena in this region reasonably

© Author(s) 2018. CC BY 4.0 License.

well, for the rough terrain in the Himalayas presents a significant challenge for modelling and the data is thus likely to suffer from biases and other deviations from the observed meteorology (Xie et al., 2007). The wind vector at 850 mb in the 20-30° N latitude band was westerly with variable wind speeds in the IGP region near the Himalayan foothills. The wind direction varies diurnally at the 850 mb level, with the wind direction shifting to southwesterly near the Himalayan foothills. Westerlies were also generally prevalent at the 500 mb; however, in the mid-latitudes between 40-50° N (Central Asia) , a trough and crest-like feature of the westerlies moving from west to east Asia is visible (also observed by Lüthi et al., 2015), which was also present prior to the study period. This wind feature was colder and more humid (see Figure S4 in the supplementary material) than the westerlies observed between 20-30° N. The meandering features (i.e., trough and crest) observed between 40-50° N affects the direction and magnitude of air masses (at 20-30° N) entering Nepal. For instance, the crest feature of the westerly was prevalent over the IGP and Nepal prior to 3rd May, transitions into the trough feature after the 3rd and continues during the study period. The prevalence of the trough was characterized by the intrusion of wind into lower latitudes as well as into the IGP, also indicated by the change in the temperature and humidity (Figure S4). The intrusions of mid-latitude air masses also influence the westerlies entering Nepal in the 20-30° N sector (Lüthi et al., 2015). As discussed later, variations in the vertical profiles of aerosols above 3000 m (a.s.l.) could be associated with variations observed in these upper layer winds.

Figure 2. Daily wind vector data at 850 and 500 mb, plotted using the NCEP NCAR reanalysis (2.5° x 2.5°) data over South Asia from 1-7th May 2016. The colors indicate the wind speed in ms^{-1}. The plots were generated using the default setup at www.esrl.noaa.gov/psd/data/composites/day/.

3.1.2. Summary of aerosol properties using AERONET measurement from 2010-2016

AERONET measurements (Holben et al., 1998) have been made in the Pokhara Valley since January 2010. The AERONET station (83.97° N, 28.18° E, 807 m a.s.l.) is approximately 1.1 km southeast from the Pokhara Regional Airport, located in the semi-urban area of Pokhara City. Cloud-screened and quality assured (level 2) data were used in the study. Gaps in the level 2 data were supplemented with level 1.5 data. The AERONET retrieval suffers in the monsoon months (June to September) due to interference by monsoon clouds in the Pokhara Valley, as indicated by the gap in Figure 2.

A combination of direct products such as aerosol optical depth (AOD) and inversion products such as fine AOD, absorption Ångstrom exponent (AAE) and volume size distribution were used for the analysis presented in this study. The typical reported uncertainty in the AERONET data products for AOD

© Author(s) 2018. CC BY 4.0 License.

(> 0.04) is approximately ±0.01 to ±0.02, and is higher for shorter wavelengths (Eck et al., 1999;Holben et al., 1998). The observed uncertainty in AOD also influences other AERONET products such as the Ångstrom exponent (AE) and the inversion products. Thus these derived products will have a higher uncertainty than the AOD (Schuster et al., 2006;Dubovik and King, 2000). Further details about the AERONET direct and inverted data products can be found in Holben et al. (2006).

AOD and ground-level PM generally correlate well (Green et al., 2009), although the strength of this association is greater with $PM_{2.5}$ (particulate matter less than 2.5 µm in aerodynamic diameter) than with PM_{10} (particulate matter less than 10 µm in aerodynamic diameter), and is also greater at moderate RH levels than in moist air. The association between PM_{10} (particulate matter less than 10 µm in aerodynamic diameter) and AOD might suffer from interference due to the mixed nature of aerosol particles, complex and changing sources of aerosols, and variable meteorological conditions (Singh et al., 2004).

In the Pokhara Valley, AOD values showed a strong seasonality in the wavelength bands between 340 and 1020 nm. The inter-annual variation in the AOD during 2010-2016 was closely associated with the enhancement in the fine-mode fraction, and to a lesser extent in the coarse mode for dust (Xu et al., 2014). The observed inter-annual variation in the AOD could be influenced by the interaction between aerosols and the mesoscale to synoptic-scale meteorology (Vinoj et al., 2014;Ram et al., 2010;Kaskaoutis et al., 2012a), as well as influences of the ENSO (El Niño southern oscillation) on West Asia and the IGP (Kim et al., 2016). AOD values were enhanced or elevated during the winter, with the aerosol load building up throughout the pre-monsoon months (AOD_{500nm}>0.6, Figure 3a, 3b, and S5) and then falling to their lowest values in the monsoon months (AOD_{500nm} ~0.2-0.3), most likely due to wet removal of aerosols. After the low AOD during the monsoon, AOD gradually increases (to ~0.4-0.5) during the post-monsoon through winter to the pre-monsoon season. AOD was usually highest in April (AOD_{500nm}:0.86±0.36), followed by March, May and June. The increase in aerosols load (as reflected by the AOD) during the pre-monsoon months can also be seen at high altitude sites such as the NCO-P site in the Khumbu Valley near Mt. Everest, located at 5057 m (a.s.l.) and about 300 km to the east of Pokhara (see Figure 3c), as well as at IGP sites in Kanpur (130 m a.s.l., 400 km southwest of the Pokhara Valley) and Gandi Nagar (60 m a.s.l., 250 km south of the Pokhara Valley). A similar AOD build-up was also observed by Ram et al. (2010) in Darjeeling (2194 m a.s.l., hill station ~450 km east of Pokhara Valley), and by Chatterjee et al. (2012) in Manora Peak (1950 m a.s.l., 460 km west of Pokhara Valley). This regional increase in aerosol load in the IGP and Himalayan region is partly due to active transport

© Author(s) 2018. CC BY 4.0 License.

during the pre-monsoon season, often linked with westerly advection bringing dust from West Asia and nearby arid regions (Gautam et al., 2011). The relatively dryness with little precipitation during this period also contributes to the total aerosol load, since washout will be limited. The AOD peaks occur in different months in these different sites in the IGP and Himalayas, reflecting the varying influence of local meteorology and increase in the emission sources such as agriculture residue burning dominated by dominated by fine-mode particles (Putero et al., 2014).

Fine-mode aerosol particles scatter more at shorter wavelengths (such as 340-500 nm) compared to 1020 nm (Schuster et al., 2006). The variation in the Ångstrom exponent was not as definitive as in the AOD values; the Ångstrom exponent was generally below 1 during pre-monsoon months and above 1 in the post-monsoon and winter months. Ångstrom exponent values of >1 are generally reported for sources such as biomass burning, fossil fuel combustion and other primary sources which have a dominant fine-mode fraction. Dust and other coarse-mode aerosols have Ångstrom exponents less than 1 (Eck et al., 1999). The highest values of the Ångstrom exponent (at least >1.2) were observed for the post-monsoon observation period, presumably due to emissions of primary fine-mode aerosol from sources such as open burning of agriculture, often reported in tshis season especially to the south and southeast of Pokhara Valley and in the IGP. In addition to the Ångstrom exponent, the temporal variation of AOD fine and coarse modes (at 500 nm) in Figure 3b and 3c also indicates that fine-mode aerosols nearly exclusively dominate the atmospheric column during the post-monsoon and winter seasons. In the pre-monsoon season, in addition to the fine-mode, a substantial fraction of coarse-mode also exists, which is also observed in the monsoon season.

On the nature of aerosols or bulk composition, Figure 3e shows a simple scatter-plot based on the absorption and extinction Ångstrom exponents (AAE and EAE at 440-870 nm) which can be used to indicate the aerosol types (Giles et al., 2011;Giles et al., 2012;Dubovik et al., 2002).These two parameters describe the spectral dependence or "slope" of aerosols absorption and extinction at the measured wavelength (Seinfeld and Pandis, 2006). Extinction exponent is a proxy for aerosol size, while the absorption exponent is a proxy for absorbing aerosols including a mixed aerosol. The classification employed by Giles et al. (2011) based on observations from the IGP AERONET sites defines *"Dust"* or "*Mostly Dust*" aerosols within the range of EAE <0.5 and AAE >2.0 and "*Mostly BC like"* aerosols with EAE EAE <0.8 and AAE ~1.0-2.0. Urban/industrial and biomass burning aerosols fall under the "Mostly BC" category (Dubovik et al., 2002;Giles et al., 2011). The mixed aerosol ("Dust+BC") centers around a value of EAE ~0.5 and AAE~1.5. Based on this approximate classification from a monthly data, the

© Author(s) 2018. CC BY 4.0 License.

dominant aerosol in the Pokhara Valley is mostly *BC like*; however, the daily aerosol characteristics can vary from more mixed to dust-like in the pre-monsoon months, to more BC-like in the post-monsoon and winter months.

Figure 3. AERONET-based aerosol optical depth and radiative properties in the Pokhara Valley from 2010 to 2016. Monthly summaries are presented using level 2 collections and supplemented with level 1.5 for missing data points; **(3a)** AOD at seven wavelengths; **(3b)** Inversion products such as fine AOD (AOD-F), coarse AOD (AOD-C), and total AOD (AOD-T), along with Ångstrom exponent (440-870 nm, magenta line); **(3c)** AOD-T for Kanpur, Gandi Nagar (both IGP sites in India) and the NCO-P site (labeled EVK2-CNR, a high altitude site in the Khumbu Valley at the base of Mt. Everest); **(3d)** Seasonal average of volume particle size distribution grouped by four seasons (the error bar indicates the standard deviation, and the uncertainty in the calculated size distribution is close to 20 % in the range 0.2 µm $<D_p<$ 14 µm). The four seasons are classified as winter (DJF: December, January and February), monsoon (JJAS: June, July, August and September), pre-monsoon (MAM: March, April and May) and post-monsoon (ON: October and November); **(3e)** absorption Ångstrom exponent (440-870) and extinction Ångstrom exponent (440-870 nm), color-coded for the four seasons

3.2. Vertical profiles of absorbing aerosols, particle number and size distribution, temperature, and dew point

The five test flights are labelled as F1-5 in Figure 4, except F3 which is shown in supplement (Fig. S10). Due to limitations of the flight permit, the test flights were conducted remaining within the Pokhara Valley as indicated by Figure 1. Among the five flights, F1, F3 and F5 were morning flights and F2 and F4 were afternoon flights.

Figure 4. Vertical profiles of aerosol species and meteorological parameters during the 5-7th May 2016 test flights in the Pokhara Valley using the IKARUS microlight aircraft. The subplot in each row is arranged by (**i**) size distribution measured by the Grimm OPC 1.108 (0.3-20 µm), limited to 1 µm in the figure, (**ii**) Total particle concentration (also indicated as ***TPC***, Dp >11 nm) measured by the CPC 3760, along with absorbing aerosol mass density at 370 nm and 880 nm (**iii**) temperature (red line, in °C) and dew point (black dots, in °C) and relative humidity (or RH %), (**iv**) calculated absorption Ångstrom exponent averaged for every 500 meters elevation band. For the size distribution plot, the x-axis represents the optical diameter of the aerosol (nm), and the color bar represents the concentration (10^x in #cm^{-3}). Of the five test flights, only F1-2, F4-5 is shown here, F3 is in the supplementary. Number size

© Author(s) 2018. CC BY 4.0 License.

356 distribution data from Flight F3 is not available due to the failure of the Grimm's pump during flight
357 initiation. In each subplot, the y-axis is the altitude above the mean sea level (in m). The origin of the y-
358 axis is at 815 m (a.s.l.).

359 All the vertical profiles of total particle concentration (also indicated as ***TPC*** in Figure 4) showed a
360 strong gradient below 2000 m (a.s.l.). Because of the valley geography, with surrounding mountains of
361 about ~2000 m (a.s.l.) or higher, it is likely that the gradient observed below 2000 m (a.s.l.) is mainly
362 caused by the primary emissions in the Pokhara Valley. The number size distribution of accumulation
363 mode aerosols (Dia. = 0.3 to 0.5 µm) and the total particle concentration (>11 nm) vary similarly as a
364 function of the altitude. Concentrations near the surface (~<1000 m a.s.l.) were generally higher than in
365 the elevated air. For example, the total particle concentrations near the surface were mostly >10^3 cm^{-3},
366 but could reach ~ 3x10^4 cm^{-3} or higher (see F5 in Figure 4) which is attributed to the coupling of the
367 shallow boundary layer and the primary emissions in the contained valley topography (Mues et al.,
368 2017). In contrast, for the afternoon flight F2 (5th May), the concentrations of accumulation-mode
369 aerosols at 2500-3000 m (a.s.l.) were higher or comparable (OPC size distribution) to the concentrations
370 observed at ~1000 m (a.s.l.). The total particle concentration at 2500-3000 m (a.s.l.) in F2 also indicated
371 a polluted air mass (5-6x10^3 cm^{-3}), clearly elevated compared to the concentrations above and below,
372 but still notably lower than the concentration at the surface (~1x10^4 cm^{-3}). The morning profile for the
373 same day (F1) showed a polluted layer above 3000-3500 m (a.s.l.), slightly higher in elevation than the
374 elevated polluted air observed in F2, but lower in particle number concentration (3-4x10^3 cm^{-3}). The
375 elevated polluted air mass in F1 and F2 could be an indication of transport related to the mountain
376 valley winds and/or synoptic transport related to the westerlies, common during this season (Gautam et
377 al., 2011;Raatikainen et al., 2014;Marcq et al., 2010). Pre-monsoon airborne measurements over the IGP
378 and near the Himalayan foothills during CALIPEX-2009 found a polluted aerosol layer (2-4x10^3 cm^{-3} of
379 0.13 µm dia. size) below 4 km (a.s.l), attributed to biomass burning observed in this particular season
380 (Padmakumari et al., 2013).
381
382 The movement of the boundary layer during the day clearly influences the evolution of the aerosol
383 vertical profile in the Pokhara Valley. The shallow boundary layer in the night which continues till the
384 morning led to the accumulation of aerosols below 2000 m (a.s.l.) in the morning profiles (see the
385 morning flights F1, F3 and F5) and a strong decrease with altitude. However, among the morning
386 profiles, substantial variations were observed (between F1 and F5); in F5 there is no polluted layer
387 above 2000 m (a.s.l.), and overall the observed number concentrations indicate cleaner atmospheric

© Author(s) 2018. CC BY 4.0 License.

388 conditions than the profile in F1. The afternoon profiles (F2 and F4) showed a more relatively mixed
389 profile up to about 2500-3000 m, decreasing then up to the maximum sampled altitude of just above
390 4,000 m (a.s.l.). Cloud layers were present at and above 4000 m (a.s.l.) in F4 (also indicated by sharp rise
391 in RH from ca. 3600 m a.s.l.), which may have led to the scavenging of the aerosol by cloud droplets and
392 thus the observed drop in the number concentration. Among primary sources in the valley contributing
393 to the aerosol concentration, open agriculture fires are common during the pre-monsoon season.
394 Occasional interception of the outflow from agriculture fires around 1500-2000 m (a.s.l.) was observed,
395 resulting in a sharp rise in the total aerosol concentration. The fire signals are clearly evident in flight F2
396 (~ 1500 m a.s.l.) and F5 (<2000 m a.s.l.).

397 The mass concentrations of absorbing aerosols estimated from aerosol absorption measurements
398 by the aethalometer at wavelengths of 880 nm (or BC) and 370 nm (indicators of the presence of
399 organic aerosols, often referred to as UVBC) are shown in Figure 4 (ngm^{-3}, second column of panels, top
400 x-axis) along with the total particle concentration (# cm^{-3}, bottom x-axis). The similarity in the vertical
401 concentration gradients of the absorbing aerosol mass concentrations and the aerosol number
402 concentration above 2000 m (a.s.l.) provides evidence of similar emission sources or origin. The BC
403 concentration was close to 1 µgm^{-3} up to 4000 m (a.s.l.) during the first two afternoon flights, but was
404 only about ~0.4 µgm^{-3} during F5. The near surface BC concentrations measured in this study were much
405 lower than surface BC concentrations measured in the pre-monsoon season (2013) in the Kathmandu
406 Valley (hourly average: ~5-40 µgm^{-3}, Mues et al. (2017)), but comparable to winter measurements
407 (2004) in Kanpur (1-3 min average: ~1-7 µgm^{-3}, Tripathi et al. (2005)). In the same study, winter-time
408 airborne measurements by Tripathi et al. (2005) observed BC concentrations close to 1 µgm^{-3} up to 2000
409 m (a.s.l.) and a sharp gradient was observed below 400 m (a.s.l.) most likely due to a shallow boundary
410 layer in winter.

411 The absorption at multiple wavelengths was used to calculate the absorption Ångstrom exponent
412 (AAE), shown in the right-most subplot in each row of Figure 4. AAE was calculated by estimating the
413 slope of the absorption coefficient ($-\frac{dln(Abs(\lambda))}{dln(\lambda)}$) at the two measured absorption wavelengths (440
414 and 880 nm, absorption as "Abs" and wavelength as "λ" in the equation). The mass absorption
415 coefficients (MAC) of 14.5 and 7.77 m^2 g^{-1}, as prescribed by the manufacturer of the aethalometer
416 (Hansen et al., 1984) for wavelength 440 nm and 880 nm, respectively were used to calculate the
417 absorption coefficient. The calculated AAE was averaged for each 500 m (a.s.l.), as shown in the figure.
418 Surface AAE was close to 0.8 to 1.2 which indicates the presence of BC from a mix of sources (biomass

© Author(s) 2018. CC BY 4.0 License.

419 burning and fossil fuel combustion. A source-diagnostic analysis of C-isotopes of elemental carbon (EC)
420 in TSP (total suspended particulates) collected in Pokhara during April 2013-March 2014 showed that
421 biomass burning and fossil fuel combustion contributes nearly 50 % each to the (annual average) EC
422 concentration (Li et al., 2016). AAE values above surface (>1000 m a.s.l.) varied from 0.5 to 2, but
423 mostly falling in the range of 0.9- 1.2, which is typically reported for mixed to *BC like* aerosols from
424 urban and industrial emissions (Russell et al., 2010;Yang et al., 2009;Dumka et al., 2014). AAE<1 could
425 also be indicative of a composite aerosol, where a BC aerosol (or "core") is coated with absorbing or
426 non-absorbing aerosols (Gyawali et al., 2009).

427 **Figure 5**. Aerosol extinction coefficient (at 532 nm) vertical profile (left) and aerosol type
428 classification based on the CALIPSO level 2 retrieval (right). Only the CALIPSO overpass over the Pokhara
429 Valley or nearby locations (such as Kathmandu Valley region, and the region to the west of Pokhara
430 Valley) is included. The extinction profile is averaged for the region 27-28.5° N latitude, which also
431 includes the Pokhara Valley. The time is in UTC.

432 The measured vertical profiles were also complemented with CALIPSO retrievals over the Pokhara
433 Valley (Figure 5). Level 2 (version 4), cloud and quality screened data were used to generate the
434 vertically resolved extinction (at 532 nm) and aerosol classification. The CALIPSO satellite had only three
435 overpasses over the Pokhara Valley between 1 and 10th May 2016 (the extinction profile lines with circle
436 markers are for the Pokhara Valley). Therefore, the satellite overpasses through nearby regions such as
437 the Kathmandu Valley region to the east and the region to the west of the Pokhara Valley (denoted by
438 *WestPV* in Figure 5) were also considered. The range of extinction values for the Pokhara Valley (0.15-
439 0.25 km^{-1} especially around 2000-4000 m a.s.l.) were similar to pre-monsoon values (0.15-3 km^{-1})
440 reported in Nainital (a hilly station located ~2000 m (a.s.l.) in India, and 400 km west of the Pokhara
441 Valley) and slightly less than Kanpur, a site in the IGP, about 400 km to the southwest of Pokhara
442 (Dumka et al., 2014). A large extinction (>0.5 km^{-1}) was observed on 1st May over the Pokhara Valley at
443 an altitude of 3-4 km (a.s.l.) which can be attributed to smoke (biomass- related) and polluted dust (a
444 mixture of dust and biomass smoke or urban pollution) as evident by the aerosol type classification.
445 Aerosols over the IGP and in the proximity of the Himalayan foothills were mainly "Dust" on 1st May.
446 Although not conclusive, the 7th May aerosol type classification is markedly different from 1st May with
447 the absence of dust in the IGP, and absence of polluted dust or smoke over the Pokhara Valley.

448 **Figure 6**. HYSPLIT (Hybrid Single Particle Lagrangian Integrated Trajectory) 3 day back trajectories of air
449 masses arriving at 3 different heights (800 m, 1500 m and 2500 m) from above the ground level (AGL~

© Author(s) 2018. CC BY 4.0 License.

450 815 m a.s.l.) in the Pokhara Valley (28.19° N, 83.98° E) during 5-7th May 2016. NCEP GDAS (Global Data
451 Assimilation System) Reanalysis data with 1°x1° horizontal resolution were used as the input
452 meteorology.

453 The measured vertical profiles and available satellite data from MODIS (See Figure S8) and CALIPSO
454 suggest that the synoptic-scale circulation were changing during the study period. The changing synoptic
455 circulation also influences the transport of polluted layer into the Pokhara Valley. The regional
456 meteorology station in the Pokhara Valley reported hazy conditions till 5th May (see Figure S6) which
457 disappeared from 6th May onwards followed by clear days with scattered clouds during the daytime and
458 thunderstorms in the afternoon. The variation in the AOD, AOD-F and Fine Mode Fraction (FMF) from
459 AERONET (only level 1.5 data were available, see Figure S7) also showed that high turbidity in the
460 atmospheric column, dominated by fine-mode aerosols before 5th May (AOD_{500nm}>2.0, FMF >0.9), which
461 declined sharply after 5th May. The variation in the horizontal visibility (or visual range) measured at the
462 meteorology station in the Pokhara Valley further indicates that the intensity of pollution declined
463 during the study period, especially starting on 5th May 2016.

464 Three day back trajectories (72 h) were generated using HYSPLIT (Hybrid Single Particle Lagrangian
465 Integrated Trajectory) for air masses arriving in the Pokhara Valley at 800 m, 1,500 m and 2,500 m from
466 above ground level (AGL) for the test flight period (see Figure 6). The NCEP GDAS reanalysis data with a
467 1°x1° horizontal resolution were used as the input meteorology for the trajectories. The majority of air
468 masses (especially at 1500 and 2000 m AGL) were westerly. A high resolution (0.0625° horizontal)
469 simulation of air mass trajectories during the pre-monsoon period over the Himalayas and Tibetan
470 Plateau region by Lüthi et al. (2015) also identified synoptic-scale transport (as westerly advection
471 around 500 mb) and a convection-enabled polluted airmass from the IGP as a major mechanism of
472 transport in the himalayas. Transport by both mechanisms was coupled with the diurnal expansion of
473 PBL height in the IGP where the trajectory height was similar to PBL height thus allowing mixing up of
474 the polluted layer, also observed by Raatikainen et al. (2014) over Gual Pahari (IGP site) and Mukteswor
475 (Himalayan foothill site).

476 During the study period, the direction of the trajectories varied as the air masses entered Nepal and
477 eventually into the Pokhara Valley. On 5th and 6th May, the air masses (at 1500 and 2000 m AGL) were
478 mostly northwesterly traversing through northern India and western Nepal before entering the Pokhara
479 Valley. A shift in the trajectory direction from north westerly to south westerly was observed on 7th May,
480 where the trajectories ware moving through central India and the southern foothills into the Pokhara

© Author(s) 2018. CC BY 4.0 License.

Valley. The observed shift in the trajectories at 1500 and 2500 m AGL was modulated by the synoptic-scale changes in the mid-latitude (over Central Asia) air masses (40-50° N) (Lüthi et al., 2015). The intrusion (in the form of a trough) of the cold and humid air masses from 40-50° N (see Figure 2) into 20-30° N occurs during the study period. As the "trough" moves eastward, it shifts the synoptic air mass at 20-30° N from north westerly to south westerly on 7th May, prior to which the synoptic air masses were north westerly. The elevated polluted layer on 5 and 6th May (or F1-F4 in Figure 4) could be the result of this modulation of the westerly. The northwesterly airmass entered Nepal via Northern India, where MODIS retrievals showed a high aerosol loading (See Figure S8), which could be mainly attributed to the numerous biomass fire events (See Figure S9) observed in North India. In addition, numerous forest fires were also reported in western Nepal during the same period. As the airmass origin shifts to south westerly on 7th May (detected during flight 5), the synoptic air mass bypasses the high AOD loading over north India and contains the cold and relatively clean air from Central Asia. This resulted in the disappearance of the polluted layer over 2000 m (a.s.l.) during flight 5.

4. Conclusion

This paper provides an overview of the pre-monsoon airborne measurement carried out with a microlight aircraft platform in the Pokhara Valley in Nepal, the first-of their-kind airborne aerosol measurements in the Himalayan foothill region. The objective of the overall airborne campaign in the Himalayan region was to quantify the vertical distribution of aerosols over a polluted mountain valley region, as well as to measure the extent of regional transport into the Himalayas. In this paper, measurements from the test flights during May 2016 are summarized. These mainly include vertical profiles of aerosol number and size distribution, multi-wavelength aerosol absorption, black carbon, total particle concentration and meteorological variables. The instrument package, designed for a microlight sampling was fitted to an IKARUS-C42 microlight aircraft. A total of five test flights were conducted between 5th and 7th May 2016, including morning and evening flights for about 1-1.5 h each, as well as vertical spirals to characterize vertical profiles of aerosols and meteorological parameters

The vertical profiles of aerosol species showed strong gradients along the atmospheric column. The observed concentration gradient was strongly influenced by the mountain valley boundary layer, which resulted in a sharp gradient below about 1500-2000 m (a.s.l.). The expansion of the boundary layer was associated with the differences in the morning and afternoon profiles. Similar vertical profiles of BC concentrations and aerosol total particle concentrations provided evidence of common emission sources or co-located origins. The observed BC concentration near the surface (~ 1000 m a.s.l.) was

© Author(s) 2018. CC BY 4.0 License.

much lower than pre-monsoon BC concentrations measured in the Kathmandu Valley, but comparable to values reported during the winter season in Kanpur in the IGP. The AAE estimates near the surface, based on the absorption value, fall in the range of 0.9-1.2, which indicates the presence of *BC like* and mixed (dust, urban, biomass) aerosols. An elevated polluted layer was observed at around 3 km (a.s.l.) over the Pokhara Valley during this study. Characterized by a strong presence of dust in the IGP and polluted continental airmasses over the Pokhara Valley, the polluted layer could be linked with the westerly synoptic circulations and regional transport from the IGP and surrounding regions. The direction of the synoptic transport entering the Himalayan foothills and into Pokhara Valley, however, was influenced by the Westerlies at mid-latitudes (40-50° N). The extent of transport can be better quantified with regional airborne measurements along the south-north transect through the region between the IGP and the Himalayan foothills at high altitudes in the Himalayas, including the Pokhara Valley. We will explore the extent of such regional transport in a subsequent publication that will be primarily based on the airborne measurements in phase II (December 2016- January 2017) in the Pokhara Valley and surrounding region. The subsequent paper will also characterize the extent of vertical transport from three different mountain valleys located at different elevations along the south-north transect.

Acknowledgements. The authors would like to thank the Ministry of Population and Environment, Nepal (www.mope.gov.np), and the Civil Aviation Authority of Nepal (https://www.caanepal.org.np) for approving this campaign in Nepal. We are grateful for funding for IASS and for this study from the German Federal Ministry for Education and Research (BMBF) and the Brandenburg Ministry for Science, Research and Culture (MWFK). We would also like to thank the NASA DAACs for the data repository of MODIS, and CALIPSO satellite and as well as NOAA for the meteorology data. Special thanks to the NASA AERONET team especially Gupta Giri for operating and maintaining the Pokhara station. The work was only possible by the support and team-work of the Pokhara Ultralight Company and their operational staff for the aircraft and air traffic management.

5. References

Aryal, D., Rosoff, Y. N., and Devkota, L. P.: A Severe Hailstorm at Pokhara: CAPE Stability Index Calculations, Journal of Geosciences and Geomatics, 3, 142-153, 2015.

Bollasina, M. A., Ming, Y., and Ramaswamy, V.: Anthropogenic Aerosols and the Weakening of the South Asian Summer Monsoon, Science, 334, 502-505, 10.1126/science.1204994, 2011.

Brauer, M., Amann, M., Burnett, R. T., Cohen, A., Dentener, F., Ezzati, M., Henderson, S. B., Krzyzanowski, M., Martin, R. V., Van Dingenen, R., van Donkelaar, A., and Thurston, G. D.: Exposure

© Author(s) 2018. CC BY 4.0 License.

544 assessment for estimation of the global burden of disease attributable to outdoor air pollution,
545 Environmental science & technology, 46, 652-660, 10.1021/es2025752, 2012.
546 Burney, J., and Ramanathan, V.: Recent climate and air pollution impacts on Indian agriculture,
547 Proceedings of the National Academy of Sciences, 111, 16319-16324, 10.1073/pnas.1317275111, 2014.
548 Chatterjee, A., Ghosh, S. K., Adak, A., Singh, A. K., Devara, P. C., and Raha, S.: Effect of dust and
549 anthropogenic aerosols on columnar aerosol optical properties over Darjeeling (2200 m asl), eastern
550 Himalayas, India, PLoS One, 7, e40286, 10.1371/journal.pone.0040286, 2012.
551 Cho, C., Kim, S. W., Rupakheti, M., Park, J. S., Panday, A., Yoon, S. C., Kim, J. H., Kim, H., Jeon, H., Sung,
552 M., Kim, B. M., Hong, S. K., Park, R. J., Rupakheti, D., Mahata, K. S., Praveen, P. S., Lawrence, M. G., and
553 Holben, B.: Wintertime aerosol optical and radiative properties in the Kathmandu Valley during the
554 SusKat-ABC field campaign, Atmos. Chem. Phys., 17, 12617-12632, 10.5194/acp-17-12617-2017, 2017.
555 Cong, Z., Kawamura, K., Kang, S., and Fu, P.: Penetration of biomass-burning emissions from South Asia
556 through the Himalayas: new insights from atmospheric organic acids, 5, 9580, 10.1038/srep09580

557 http://dharmasastra.live.cf.private.springer.com/articles/srep09580#supplementary-information, 2015.
558 Decesari, S., Facchini, M. C., Carbone, C., Giulianelli, L., Rinaldi, M., Finessi, E., Fuzzi, S., Marinoni, A.,
559 Cristofanelli, P., Duchi, R., Bonasoni, P., Vuillermoz, E., Cozic, J., Jaffrezo, J. L., and Laj, P.: Chemical
560 composition of PM₁₀ and PM₁ at the high-altitude Himalayan station Nepal
561 Climate Observatory-Pyramid (NCO-P) (5079 m a.s.l.), Atmos. Chem. Phys., 10, 4583-4596, 10.5194/acp-
562 10-4583-2010, 2010.
563 Dey, S., and Di Girolamo, L.: A climatology of aerosol optical and microphysical properties over the
564 Indian subcontinent from 9 years (2000–2008) of Multiangle Imaging Spectroradiometer (MISR) data,
565 Journal of Geophysical Research: Atmospheres, 115, n/a-n/a, 10.1029/2009JD013395, 2010.
566 Dubovik, O., and King, M. D.: A flexible inversion algorithm for retrieval of aerosol optical properties
567 from Sun and sky radiance measurements, Journal of Geophysical Research: Atmospheres, 105, 20673-
568 20696, 10.1029/2000JD900282, 2000.
569 Dubovik, O., Holben, B., Eck, T. F., Smirnov, A., Kaufman, Y. J., King, M. D., Tanré, D., and Slutsker, I.:
570 Variability of Absorption and Optical Properties of Key Aerosol Types Observed in Worldwide Locations,
571 Journal of the Atmospheric Sciences, 59, 590-608, 10.1175/1520-0469(2002)059<0590:voaaop>2.0.co;2,
572 2002.
573 Dumka, U. C., N. Tripathi, S., Misra, A., Giles, D. M., Eck, T. F., Sagar, R., and Holben, B. N.: Latitudinal
574 variation of aerosol properties from Indo-Gangetic Plain to central Himalayan foothills during TIGERZ
575 campaign, Journal of Geophysical Research: Atmospheres, 119, 4750-4769, 10.1002/2013jd021040,
576 2014.
577 Eck, T. F., Holben, B. N., Reid, J. S., Dubovik, O., Smirnov, A., O'Neill, N. T., Slutsker, I., and Kinne, S.:
578 Wavelength dependence of the optical depth of biomass burning, urban, and desert dust aerosols,
579 Journal of Geophysical Research: Atmospheres, 104, 31333-31349, 10.1029/1999JD900923, 1999.
580 Gautam, R., Hsu, N. C., Lau, K. M., and Kafatos, M.: Aerosol and rainfall variability over the Indian
581 monsoon region: distributions, trends and coupling, Ann. Geophys., 27, 3691-3703, 10.5194/angeo-27-
582 3691-2009, 2009a.
583 Gautam, R., Hsu, N. C., Lau, K. M., Tsay, S. C., and Kafatos, M.: Enhanced pre-monsoon warming over the
584 Himalayan-Gangetic region from 1979 to 2007, Geophysical Research Letters, 36, n/a-n/a,
585 10.1029/2009GL037641, 2009b.
586 Gautam, R., Hsu, N. C., Tsay, S. C., Lau, K. M., Holben, B., Bell, S., Smirnov, A., Li, C., Hansell, R., Ji, Q.,
587 Payra, S., Aryal, D., Kayastha, R., and Kim, K. M.: Accumulation of aerosols over the Indo-Gangetic plains
588 and southern slopes of the Himalayas: distribution, properties and radiative effects during the 2009 pre-
589 monsoon season, Atmospheric Chemistry and Physics, 11, 12841-12863, 10.5194/acp-11-12841-2011,
590 2011.

© Author(s) 2018. CC BY 4.0 License.

591 Giles, D. M., Holben, B. N., Tripathi, S. N., Eck, T. F., Newcomb, W. W., Slutsker, I., Dickerson, R. R.,
592 Thompson, A. M., Mattoo, S., Wang, S.-H., Singh, R. P., Sinyuk, A., and Schafer, J. S.: Aerosol properties
593 over the Indo-Gangetic Plain: A mesoscale perspective from the TIGERZ experiment, Journal of
594 Geophysical Research, 116, 10.1029/2011jd015809, 2011.
595 Giles, D. M., Holben, B. N., Eck, T. F., Sinyuk, A., Smirnov, A., Slutsker, I., Dickerson, R. R., Thompson, A.
596 M., and Schafer, J. S.: An analysis of AERONET aerosol absorption properties and classifications
597 representative of aerosol source regions, Journal of Geophysical Research: Atmospheres, 117, n/a-n/a,
598 10.1029/2012jd018127, 2012.
599 Gogoi, M. M., Moorthy, K. K., Kompalli, S. K., Chaubey, J. P., Babu, S. S., Manoj, M. R., Nair, V. S., and
600 Prabhu, T. P.: Physical and optical properties of aerosols in a free tropospheric environment: Results
601 from long-term observations over western trans-Himalayas, Atmospheric Environment, 84, 262-274,
602 https://doi.org/10.1016/j.atmosenv.2013.11.029, 2014.
603 Green, M., Kondragunta, S., Ciren, P., and Xu, C.: Comparison of GOES and MODIS Aerosol Optical Depth
604 (AOD) to Aerosol Robotic Network (AERONET) AOD and IMPROVE PM2.5 Mass at Bondville, Illinois,
605 Journal of the Air & Waste Management Association, 59, 1082-1091, 10.3155/1047-3289.59.9.1082,
606 2009.
607 Guttikunda, S. K., Goel, R., and Pant, P.: Nature of air pollution, emission sources, and management in
608 the Indian cities, Atmospheric Environment, 95, 501-510,
609 http://dx.doi.org/10.1016/j.atmosenv.2014.07.006, 2014.
610 Gyawali, M., Arnott, W. P., Lewis, K., and Moosmüller, H.: In situ aerosol optics in Reno, NV, USA during
611 and after the summer 2008 California wildfires and the influence of absorbing and non-absorbing
612 organic coatings on spectral light absorption, Atmos. Chem. Phys., 9, 8007-8015, 10.5194/acp-9-8007-
613 2009, 2009.
614 Hansen, A. D. A., Rosen, H., and Novakov, T.: The aethalometer — An instrument for the real-time
615 measurement of optical absorption by aerosol particles, Science of The Total Environment, 36, 191-196,
616 https://doi.org/10.1016/0048-9697(84)90265-1, 1984.
617 Holben, B. N., Eck, T. F., Slutsker, I., Tanré, D., Buis, J. P., Setzer, A., Vermote, E., Reagan, J. A., Kaufman,
618 Y. J., Nakajima, T., Lavenu, F., Jankowiak, I., and Smirnov, A.: AERONET—A Federated Instrument
619 Network and Data Archive for Aerosol Characterization, Remote Sensing of Environment, 66, 1-16,
620 http://dx.doi.org/10.1016/S0034-4257(98)00031-5, 1998.
621 Jai Devi, J., Tripathi, S. N., Gupta, T., Singh, B. N., Gopalakrishnan, V., and Dey, S.: Observation-based 3-D
622 view of aerosol radiative properties over Indian Continental Tropical Convergence Zone: implications to
623 regional climate, Tellus B, 63, 971-989, 10.1111/j.1600-0889.2011.00580.x, 2011.
624 Junkermann, W.: An Ultralight Aircraft as Platform for Research in the Lower Troposphere: System
625 Performance and First Results from Radiation Transfer Studies in Stratiform Aerosol Layers and Broken
626 Cloud Conditions, Journal of Atmospheric and Oceanic Technology, 18, 934-946, 10.1175/1520-
627 0426(2001)018<0934:auaapf>2.0.co;2, 2001.
628 Kaskaoutis, D. G., Gautam, R., Singh, R. P., Houssos, E. E., Goto, D., Singh, S., Bartzokas, A., Kosmopoulos,
629 P. G., Sharma, M., Hsu, N. C., Holben, B. N., and Takemura, T.: Influence of anomalous dry conditions on
630 aerosols over India: Transport, distribution and properties, Journal of Geophysical Research:
631 Atmospheres, 117, n/a-n/a, 10.1029/2011JD017314, 2012a.
632 Kaskaoutis, D. G., Singh, R. P., Gautam, R., Sharma, M., Kosmopoulos, P. G., and Tripathi, S. N.: Variability
633 and trends of aerosol properties over Kanpur, northern India using AERONET data (2001–10),
634 Environmental Research Letters, 7, 024003, 10.1088/1748-9326/7/2/024003, 2012b.
635 Khadka, U. R., and Ramanathan, A.: Major ion composition and seasonal variation in the Lesser
636 Himalayan lake: case of Begnas Lake of the Pokhara Valley, Nepal, Arabian Journal of Geosciences, 6,
637 4191-4206, 10.1007/s12517-012-0677-4, 2013.

© Author(s) 2018. CC BY 4.0 License.

638 Kim, M.-K., Lau, W. K. M., Kim, K.-M., Sang, J., Kim, Y.-H., and Lee, W.-S.: Amplification of ENSO effects
639 on Indian summer monsoon by absorbing aerosols, Climate Dynamics, 46, 2657-2671, 10.1007/s00382-
640 015-2722-y, 2016.
641 Kuhlmann, J., and Quaas, J.: How can aerosols affect the Asian summer monsoon? Assessment during
642 three consecutive pre-monsoon seasons from CALIPSO satellite data, Atmos. Chem. Phys., 10, 4673-
643 4688, 10.5194/acp-10-4673-2010, 2010.
644 Lau, W.: Atmospheric science: Desert dust and monsoon rain, Nature Geosci, 7, 255-256,
645 10.1038/ngeo2115, 2014.
646 Lawrence, M. G., and Lelieveld, J.: Atmospheric pollutant outflow from southern Asia: a review, Atmos.
647 Chem. Phys., 10, 11017-11096, 10.5194/acp-10-11017-2010, 2010.
648 Li, C., Bosch, C., Kang, S., Andersson, A., Chen, P., Zhang, Q., Cong, Z., Chen, B., Qin, D., and Gustafsson,
649 O.: Sources of black carbon to the Himalayan-Tibetan Plateau glaciers, Nat Commun, 7, 12574,
650 10.1038/ncomms12574, 2016.
651 Lüthi, Z. L., Škerlak, B., Kim, S. W., Lauer, A., Mues, A., Rupakheti, M., and Kang, S.: Atmospheric brown
652 clouds reach the Tibetan Plateau by crossing the Himalayas, Atmos. Chem. Phys., 15, 6007-6021,
653 10.5194/acp-15-6007-2015, 2015.
654 Marcq, S., Laj, P., Roger, J. C., Villani, P., Sellegri, K., Bonasoni, P., Marinoni, A., Cristofanelli, P., Verza, G.
655 P., and Bergin, M.: Aerosol optical properties and radiative forcing in the high Himalaya based on
656 measurements at the Nepal Climate Observatory-Pyramid site (5079 m a.s.l.), Atmos. Chem. Phys., 10,
657 5859-5872, 10.5194/acp-10-5859-2010, 2010.
658 Marinoni, A., Cristofanelli, P., Laj, P., Duchi, R., Putero, D., Calzolari, F., Landi, T. C., Vuillermoz, E.,
659 Maione, M., and Bonasoni, P.: High black carbon and ozone concentrations during pollution transport in
660 the Himalayas: Five years of continuous observations at NCO-P global GAW station, Journal of
661 Environmental Sciences, 25, 1618-1625, http://dx.doi.org/10.1016/S1001-0742(12)60242-3, 2013.
662 Mues, A., Rupakheti, M., Münkel, C., Lauer, A., Bozem, H., Hoor, P., Butler, T., and Lawrence, M. G.:
663 Investigation of the mixing layer height derived from ceilometer measurements in the Kathmandu Valley
664 and implications for local air quality, Atmos. Chem. Phys., 17, 8157-8176, 10.5194/acp-17-8157-2017,
665 2017.
666 Padmakumari, B., Maheskumar, R. S., Morwal, S. B., Harikishan, G., Konwar, M., Kulkarni, J. R., and
667 Goswami, B. N.: Aircraft observations of elevated pollution layers near the foothills of the Himalayas
668 during CAIPEEX-2009, Quarterly Journal of the Royal Meteorological Society, 139, 625-638,
669 10.1002/qj.1989, 2013.
670 Panday, A. K., and Prinn, R. G.: Diurnal cycle of air pollution in the Kathmandu Valley, Nepal:
671 Observations, Journal of Geophysical Research: Atmospheres, 114, D09305, 10.1029/2008JD009777,
672 2009.
673 Pandey, S. K., Vinoj, V., Landu, K., and Babu, S. S.: Declining pre-monsoon dust loading over South Asia:
674 Signature of a changing regional climate, Scientific Reports, 7, 16062, 10.1038/s41598-017-16338-w,
675 2017.
676 Poudyal, K. N., Bhattarai, B. K., Sapkota, B. K., Kjeldstad, B., and Karki, N. R.: Estimation of Global Solar
677 Radiation using Pyranometer and NILU-UV Irradiance Meter at Pokhara Valley in Nepal, 2014, 9, 10,
678 10.3126/jie.v9i1.10672, 2014.
679 Putero, D., Landi, T. C., Cristofanelli, P., Marinoni, A., Laj, P., Duchi, R., Calzolari, F., Verza, G. P., and
680 Bonasoni, P.: Influence of open vegetation fires on black carbon and ozone variability in the southern
681 Himalayas (NCO-P, 5079 m a.s.l.), Environ Pollut, 184, 597-604, 10.1016/j.envpol.2013.09.035, 2014.
682 Putero, D., Cristofanelli, P., Marinoni, A., Adhikary, B., Duchi, R., Shrestha, S. D., Verza, G. P., Landi, T. C.,
683 Calzolari, F., Busetto, M., Agrillo, G., Biancofiore, F., Di Carlo, P., Panday, A. K., Rupakheti, M., and
684 Bonasoni, P.: Seasonal variation of ozone and black carbon observed at Paknajol, an urban site in the
685 Kathmandu Valley, Nepal, Atmos. Chem. Phys., 15, 13957-13971, 10.5194/acp-15-13957-2015, 2015.

© Author(s) 2018. CC BY 4.0 License.

686 Raatikainen, T., Hyvärinen, A. P., Hatakka, J., Panwar, T. S., Hooda, R. K., Sharma, V. P., and Lihavainen,
687 H.: The effect of boundary layer dynamics on aerosol properties at the Indo-Gangetic plains and at the
688 foothills of the Himalayas, Atmospheric Environment, 89, 548-555, 10.1016/j.atmosenv.2014.02.058,
689 2014.
690 Ram, K., Sarin, M. M., and Hegde, P.: Long-term record of aerosol optical properties and chemical
691 composition from a high-altitude site (Manora Peak) in Central Himalaya, Atmos. Chem. Phys., 10,
692 11791-11803, 10.5194/acp-10-11791-2010, 2010.
693 Ramana, M. V., Ramanathan, V., Podgorny, I. A., Pradhan, B. B., and Shrestha, B.: The direct
694 observations of large aerosol radiative forcing in the Himalayan region, Geophysical Research Letters,
695 31, n/a-n/a, 10.1029/2003GL018824, 2004.
696 Ramanathan, V., Crutzen, P. J., Kiehl, J. T., and Rosenfeld, D.: Aerosols, Climate, and the Hydrological
697 Cycle, Science, 294, 2119-2124, 10.1126/science.1064034, 2001.
698 Russell, P. B., Bergstrom, R. W., Shinozuka, Y., Clarke, A. D., DeCarlo, P. F., Jimenez, J. L., Livingston, J. M.,
699 Redemann, J., Dubovik, O., and Strawa, A.: Absorption Angstrom Exponent in AERONET and related data
700 as an indicator of aerosol composition, Atmos. Chem. Phys., 10, 1155-1169, 10.5194/acp-10-1155-2010,
701 2010.
702 Schuster, G. L., Dubovik, O., and Holben, B. N.: Angstrom exponent and bimodal aerosol size
703 distributions, Journal of Geophysical Research: Atmospheres, 111, n/a-n/a, 10.1029/2005JD006328,
704 2006.
705 Seinfeld, J. H., and Pandis, S. N.: Atmospheric Chemistry and Physics 2ed., John Wiley and Sons, New
706 Jersey, 2006.
707 Shrestha, P., Barros, A. P., and Khlystov, A.: Chemical composition and aerosol size distribution of the
708 middle mountain range in the Nepal Himalayas during the 2009 pre-monsoon season, Atmospheric
709 Chemistry and Physics, 10, 11605-11621, 2010.
710 Shrestha, P., Barros, A. P., and Khlystov, A.: CCN estimates from bulk hygroscopic growth factors of
711 ambient aerosols during the pre-monsoon season over Central Nepal, Atmospheric Environment, 67,
712 120-129, http://dx.doi.org/10.1016/j.atmosenv.2012.10.042, 2013.
713 Singh, R. P., Dey, S., Tripathi, S. N., Tare, V., and Holben, B.: Variability of aerosol parameters over
714 Kanpur, northern India, Journal of Geophysical Research: Atmospheres, 109, 10.1029/2004jd004966,
715 2004.
716 Stone, E. A., Schauer, J. J., Pradhan, B. B., Dangol, P. M., Habib, G., Venkataraman, C., and Ramanathan,
717 V.: Characterization of emissions from South Asian biofuels and application to source apportionment of
718 carbonaceous aerosol in the Himalayas, Journal of Geophysical Research: Atmospheres, 115, n/a-n/a,
719 10.1029/2009JD011881, 2010.
720 Tripathi, S. N., Dey, S., Tare, V., Satheesh, S. K., Lal, S., and Venkataramani, S.: Enhanced layer of black
721 carbon in a north Indian industrial city, Geophysical Research Letters, 32, n/a-n/a,
722 10.1029/2005gl022564, 2005.
723 Venkataraman, C., Habib, G., Kadamba, D., Shrivastava, M., Leon, J. F., Crouzille, B., Boucher, O., and
724 Streets, D. G.: Emissions from open biomass burning in India: Integrating the inventory approach with
725 high-resolution Moderate Resolution Imaging Spectroradiometer (MODIS) active-fire and land cover
726 data, Global Biogeochemical Cycles, 20, n/a-n/a, 10.1029/2005GB002547, 2006.
727 Venzac, H., Sellegri, K., Laj, P., Villani, P., Bonasoni, P., Marinoni, A., Cristofanelli, P., Calzolari, F., Fuzzi,
728 S., Decesari, S., Facchini, M. C., Vuillermoz, E., and Verza, G. P.: High frequency new particle formation in
729 the Himalayas, Proc Natl Acad Sci U S A, 105, 15666-15671, 10.1073/pnas.0801355105, 2008.
730 Vinoj, V., Rasch, P. J., Wang, H., Yoon, J.-H., Ma, P.-L., Landu, K., and Singh, B.: Short-term modulation of
731 Indian summer monsoon rainfall by West Asian dust, Nature Geosci, 7, 308-313, 10.1038/ngeo2107

732 http://www.nature.com/ngeo/journal/v7/n4/abs/ngeo2107.html#supplementary-information, 2014.

© Author(s) 2018. CC BY 4.0 License.

733 Xie, A., Ren, J., Qin, X., and Kang, S.: Reliability of NCEP/NCAR reanalysis data in the Himalayas/Tibetan
734 Plateau, Journal of Geographical Sciences, 17, 421-430, 10.1007/s11442-007-0421-2, 2007.
735 Xu, C., Ma, Y. M., Panday, A., Cong, Z. Y., Yang, K., Zhu, Z. K., Wang, J. M., Amatya, P. M., and Zhao, L.:
736 Similarities and differences of aerosol optical properties between southern and northern sides of the
737 Himalayas, Atmos. Chem. Phys., 14, 3133-3149, 10.5194/acp-14-3133-2014, 2014.
738 Yang, M., Howell, S. G., Zhuang, J., and Huebert, B. J.: Attribution of aerosol light absorption to black
739 carbon, brown carbon, and dust in China – interpretations of atmospheric measurements during EAST-
740 AIRE, Atmos. Chem. Phys., 9, 2035-2050, 10.5194/acp-9-2035-2009, 2009.

741

742

© Author(s) 2018. CC BY 4.0 License.

743 **List of Tables**

744 Table 1. Instrument package deployed in the microlight aircraft

Parameters	Instruments	Method	Sampling time resolution
1. Particle size distribution (0.3 - 20 µm)	GRIMM 1.108	Light scattering	6 s
2. Total particle concentration (>11 nm)	TSI CPC 3760	Condensation/light scattering	1 s
3. Aerosol spectral absorption	Magee AE42	7 wavelengths, light attenuation	2 min
4. Dew point sensor	METEOLABOR, TPS3	Chilled Mirror	1 Hz
5. Temperature	Thermocouple	-	1 Hz
6. Data acquisition system	PC 104+ GPS	---	---
7. Power supply	Aircraft battery pack, $LiFEPO_4$ battery	12 V, >15 AH	

745

Atmos. Chem. Phys. Discuss., https://doi.org/10.5194/acp-2018-95
Manuscript under review for journal Atmos. Chem. Phys.
Discussion started: 3 April 2018
© Author(s) 2018. CC BY 4.0 License.

Atmospheric Chemistry and Physics Discussions

746 **List of Figures**

747

748

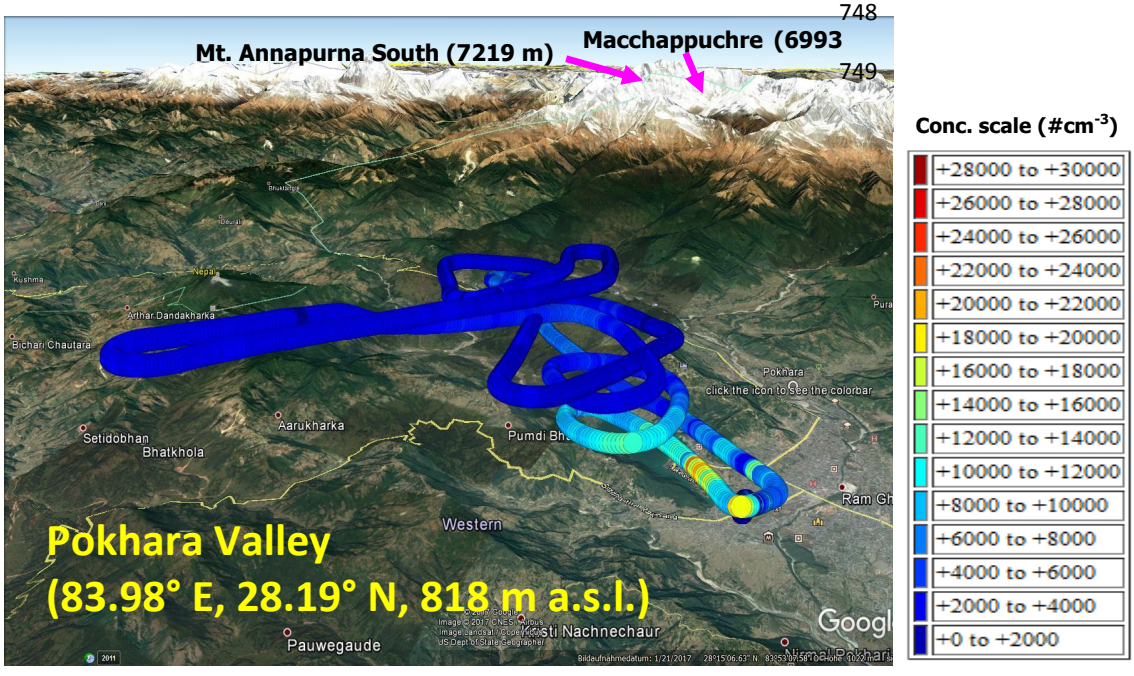

750

751 **Figure 1.** A typical test flight within the Pokhara Valley on 5th May 2017. The plot is generated using a
752 Matlab-Google Earth toolbox (https://www.mathworks.com/matlabcentral/fileexchange/12954-google-
753 earth-toolbox). Each dot is a single sample point (sampling frequency of 1Hz) and the color of the dot
754 indicates the total aerosol concentration (in # cm^{-3}) and the value of each color is shown as a color bar.

Atmos. Chem. Phys. Discuss., https://doi.org/10.5194/acp-2018-95
Manuscript under review for journal Atmos. Chem. Phys.
Discussion started: 3 April 2018
© Author(s) 2018. CC BY 4.0 License.

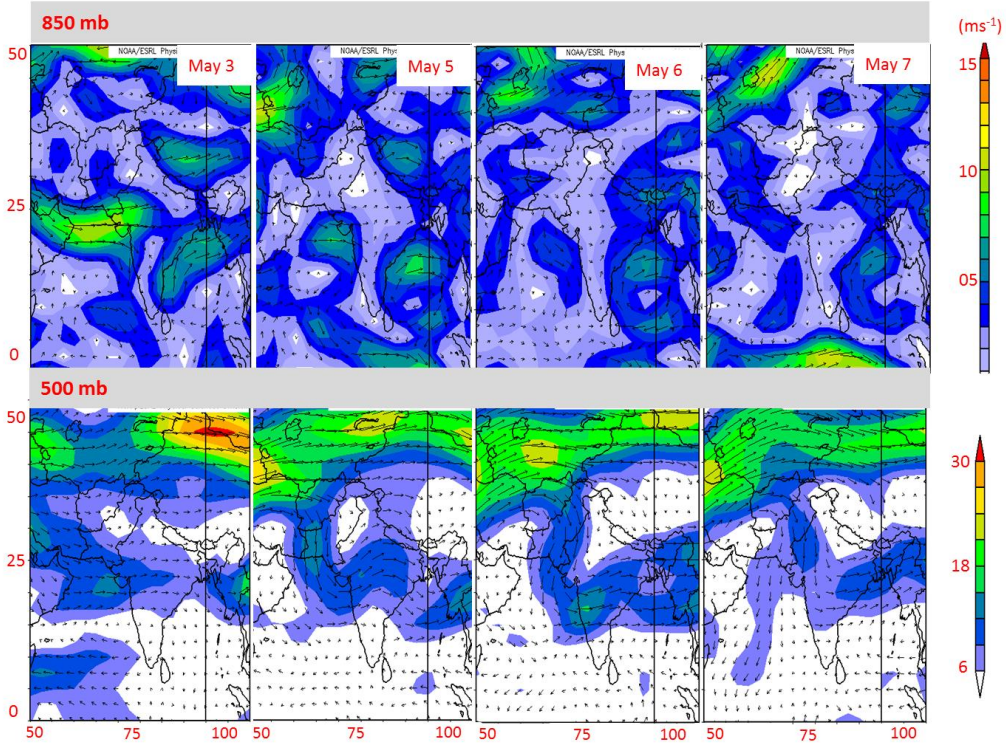

Figure 2. Daily wind vector data at 850 and 500 mb plotted using the NCEP NCAR reanalysis (2.5° x 2.5°) data over South Asia from 1-7th May 2016. The colors indicate the wind speed in ms^{-1}. The plots were generated using the default set-up at www.esrl.noaa.gov/psd/data/composites/day/.

Atmos. Chem. Phys. Discuss., https://doi.org/10.5194/acp-2018-95
Manuscript under review for journal Atmos. Chem. Phys.
Discussion started: 3 April 2018
© Author(s) 2018. CC BY 4.0 License.

Atmospheric Chemistry and Physics Discussions

759

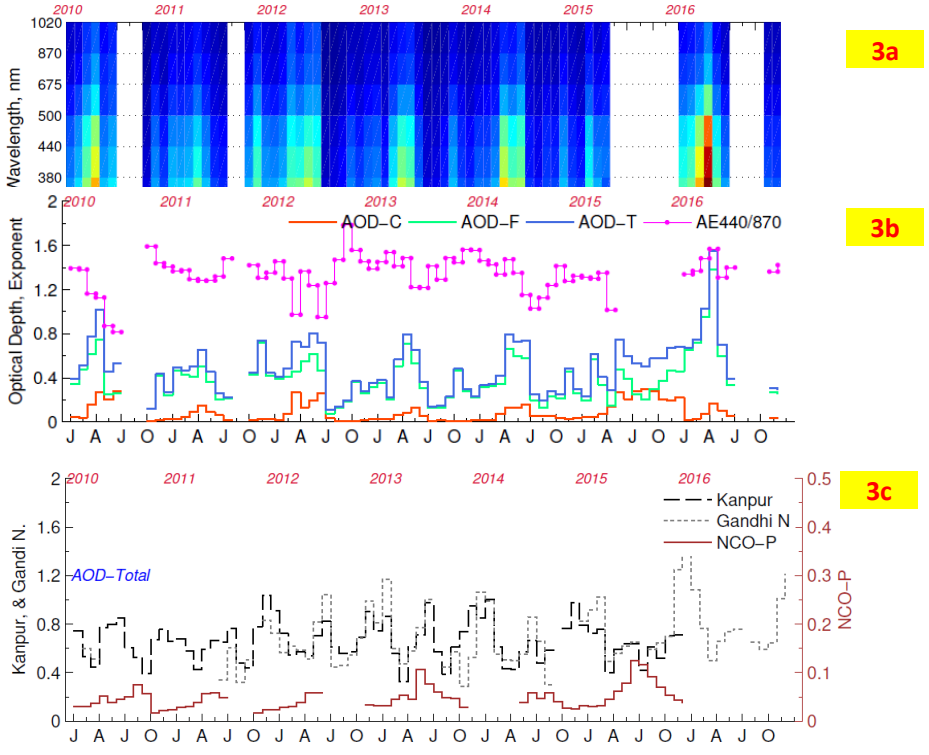

Atmos. Chem. Phys. Discuss., https://doi.org/10.5194/acp-2018-95
Manuscript under review for journal Atmos. Chem. Phys.
Discussion started: 3 April 2018
© Author(s) 2018. CC BY 4.0 License.

Atmospheric Chemistry and Physics Discussions

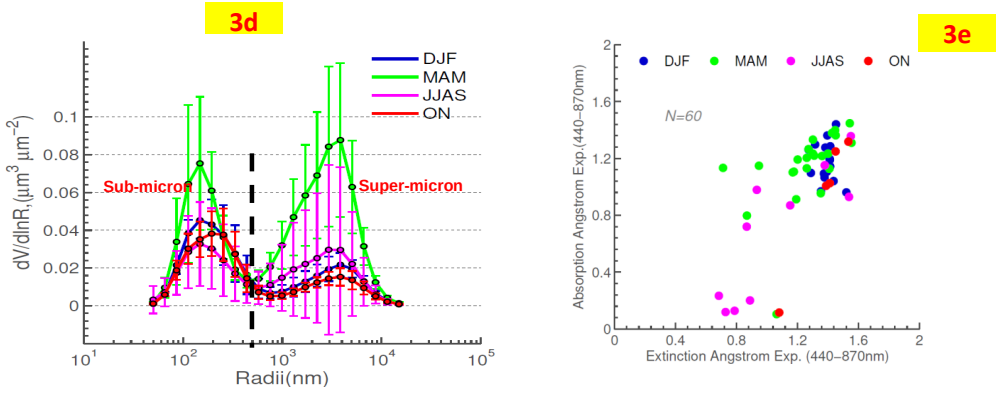

Figure 3. AERONET-based aerosol optical and radiative properties in the Pokhara Valley from 2010 to 2016. Monthly summaries are presented using level 2 collections and supplemented with level 1.5 for missing data points; **(3a)** AOD at seven wavelengths; **(3b)** Inversion products such as fine AOD (AOD-F), coarse AOD (AOD-C), and total AOD (AOD-T), along with Ångstrom exponent (440-870 nm, magenta line); **(3c)** AOD-T for Kanpur, Gandi Nagar (both IGP sites in India) and NCO-P site (high altitude site in in the Khumbu Valley in the Himalayas in Nepal); **(3d)** Seasonal average of volume particle size distribution grouped by four seasons (The error bar indicates the standard deviation, and uncertainty in the calculated size distribution is close to 20 % in the range 0.2 μm <D_p< 14 μm). The four seasons are classified as winter (DJF: December, January and February), monsoon (JJAS: June, July, August and September), pre-monsoon (MAM: March, April and May) and post-monsoon (ON: October and November); **(3e)** absorption Ångstrom exponent (440-870) and extinction Ångstrom exponent (440-870 nm) grouped by four seasons

Atmos. Chem. Phys. Discuss., https://doi.org/10.5194/acp-2018-95
Manuscript under review for journal Atmos. Chem. Phys.
Discussion started: 3 April 2018
© Author(s) 2018. CC BY 4.0 License.

Atmospheric Chemistry and Physics Discussions

779 **Figure 4**

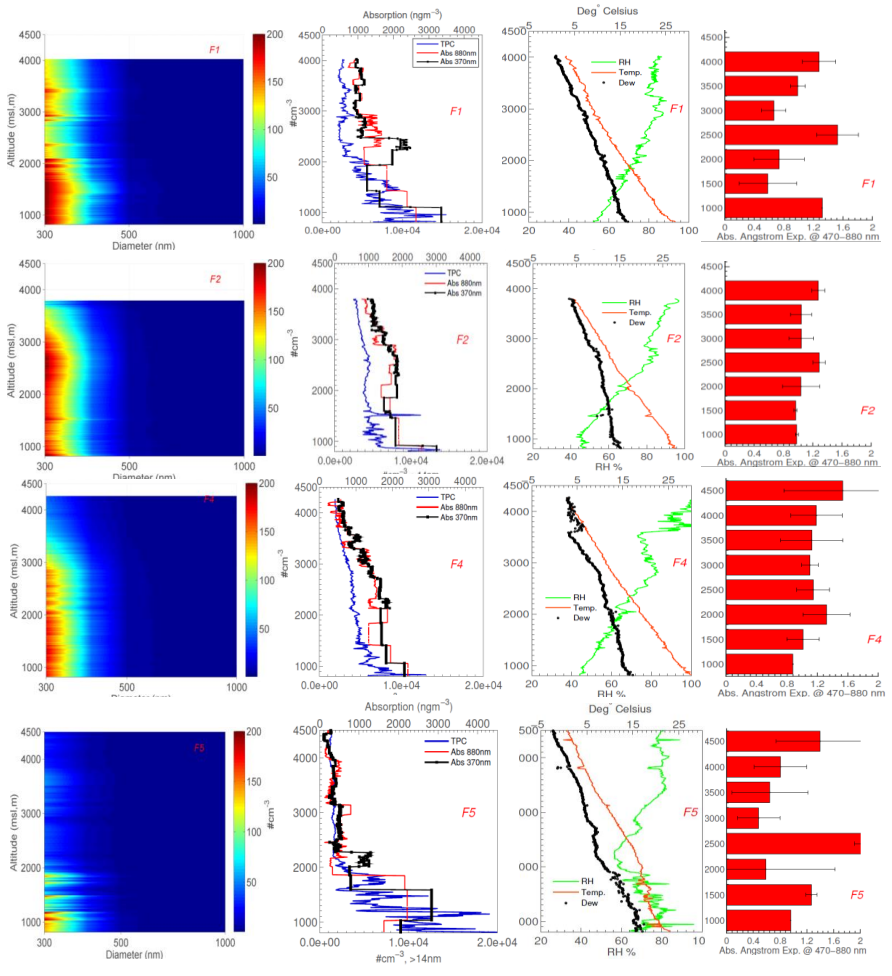

© Author(s) 2018. CC BY 4.0 License.

795 **Figure 4.** Vertical profiles of aerosol species and meteorological parameters during the 5-7th May 2016 test flights in the Pokhara Valley using
796 the IKARUS microlight aircraft. The subplot in each row is arranged by (**i**) size distribution measured by the Grimm OPC 1.108 (0.3-20 µm), limited
797 to 1 µm in the figure, (**ii**) Total particle concentration (also indicated as ***TPC***, Dp >11 nm) measured by the CPC 3760 and absorption aerosol at
798 370 nm and 880 nm (**iii**) temperature (°C) and dew point (black dot, in °C) and relative humidity (or RH %), (**iv**) calculated absorption Ångstrom
799 exponent averaged for every 500 meters elevation band. For the size distribution plot, the x-axis represents the optical diameter of the aerosol
800 (nm), and the color bar represents the concentration (10^x in #cm^{-3}). Of the five test flights, only F1-2, F4-5 is shown here, F3 is in the
801 supplementary. Number size distribution data from Flight F3 is not available due to the failure of the Grimm's pump during flight initiation. In
802 each subplot, the y-axis is the altitude above the mean sea level (in m). The origin of the y-axis is at 815 m (a.s.l.).

803

804

805

Atmos. Chem. Phys. Discuss., https://doi.org/10.5194/acp-2018-95
Manuscript under review for journal Atmos. Chem. Phys.
Discussion started: 3 April 2018
© Author(s) 2018. CC BY 4.0 License.

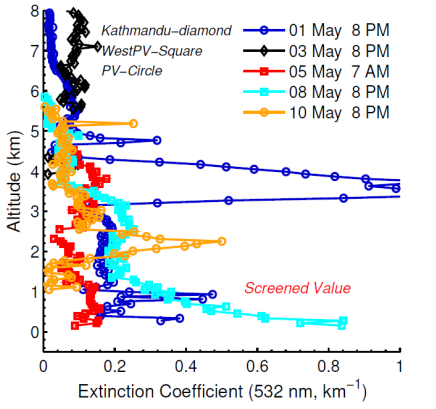

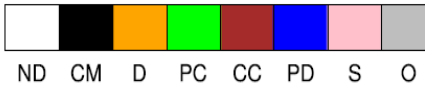

ND-not detected, **CM**: clean Marine, **D**:dust
PC: Polluted Continental, PD: Polluted Dust;
CC: clean continental, S: Smoke, **O**:Others

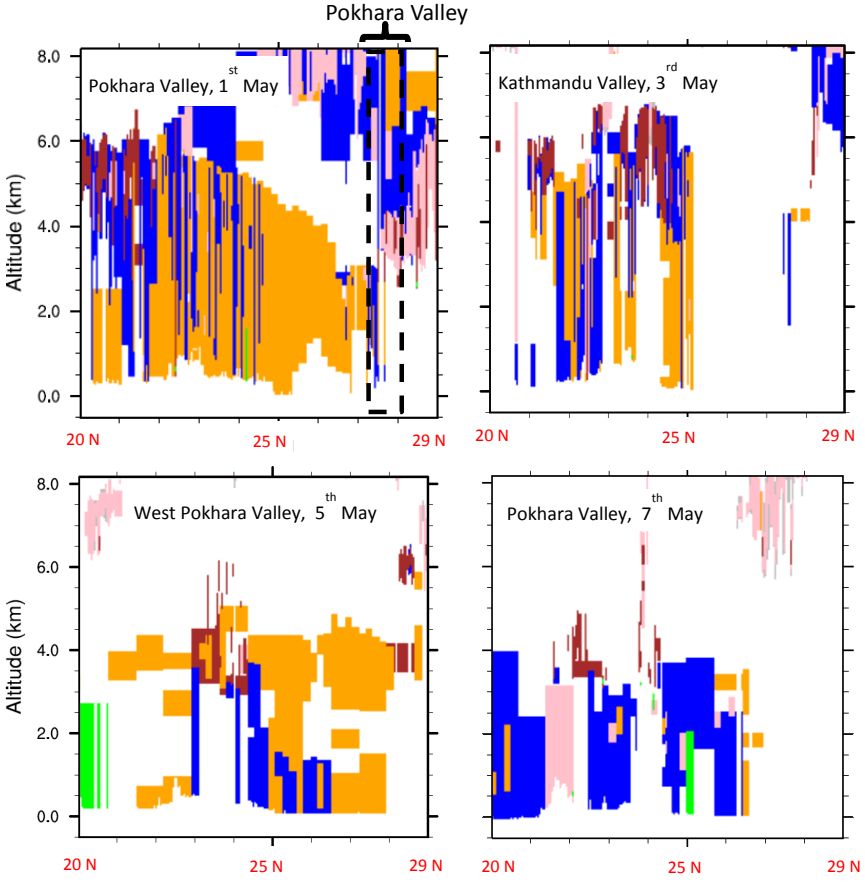

806

Atmos. Chem. Phys. Discuss., https://doi.org/10.5194/acp-2018-95
Manuscript under review for journal Atmos. Chem. Phys.
Discussion started: 3 April 2018
© Author(s) 2018. CC BY 4.0 License.

Atmospheric Chemistry and Physics Discussions

807 **Figure 5**. Aerosol extinction coefficient (at 532 nm) vertical profile (left) and aerosol type classification based on the CALIPSO level 2 retrieval
808 (right). Only the CALIPSO overpass over the Pokhara Valley or nearby locations (such as Kathmandu Valley region, and the region to west of
809 Pokhara Valley) are included). The extinction profile is averaged for the region 27-28.5° N latitude which also includes the Pokhara Valley. The
810 time is in UTC

811

Atmos. Chem. Phys. Discuss., https://doi.org/10.5194/acp-2018-95
Manuscript under review for journal Atmos. Chem. Phys.
Discussion started: 3 April 2018
© Author(s) 2018. CC BY 4.0 License.

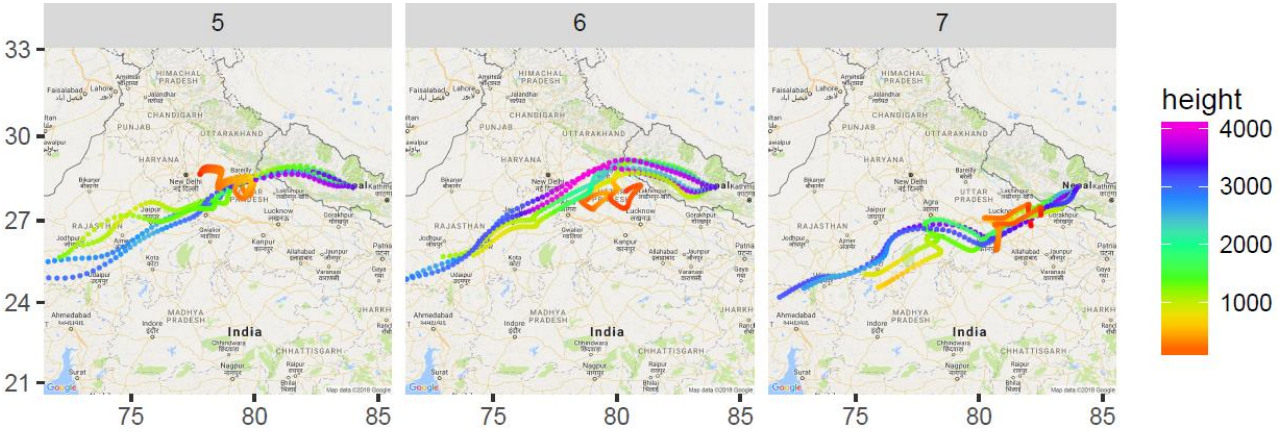

812

813 **Figure 6**. HYSPLIT (Hybrid Single Particle Lagrangian Integrated Trajectory) 3 day back trajectories of air masses arriving at 3 different heights
814 (800 m, 1,500 m and 2,500 m) from above ground level (AGL~ 815 m a.s.l.) in the Pokhara Valley during 5-7th May 2016. NCEP GDAS (Global Data
815 Assimilation System) Reanalysis data with 1°x1° horizontal resolution were used as the input meteorology.

816

817